



This discussion paper is/has been under review for the journal Climate of the Past (CP).
Please refer to the corresponding final paper in CP if available.

Tracking atmospheric and riverine terrigenous supplies variability during the last glacial and the Holocene in central Mediterranean

V. Bout-Roumazeilles¹, N. Combourieu-Nebout², S. Desprat³, G. Siani⁴, and J.-L. Turon⁵

¹Géosystèmes, UMR8217, CNRS – Université Lille 1, 59655 Villeneuve d'Ascq, France

²Laboratoire des Sciences du Climat et de l'Environnement, laboratoire Mixte CNRS-CEA-UVSQ, Avenue de la Terrasse, 91198 Gif-sur-Yvette Cedex, France

³Ecole Pratique des Hautes Etudes, Environnements et Paléoenvironnements Océaniques, UMR5808, CNRS – EPOC, Université Bordeaux I, 33405 Talence, France

⁴Laboratoire des Interactions et Dynamique des Environnements de Surface (IDES), UMR8148, CNRS – Université de Paris-Sud, Bât 504, 91405 Orsay Cedex, France

⁵Environnements et Paléoenvironnements Océaniques, UMR5808, CNRS – EPOC, Université Bordeaux I, 33405 Talence, France

Received: 12 July 2012 – Accepted: 17 July 2012 – Published: 27 July 2012

Correspondence to: V. Bout-Roumazeilles (viviane.bout@univ-lille1.fr)

Published by Copernicus Publications on behalf of the European Geosciences Union.

Abstract

CPD

8, 2921–2968, 2012

The objectives were to retrace the eolian and fluvial terrigenous supplies in a sediment core from the Sicilian-Tunisian Strait by coupling mineralogical, grain-size and geochemical approaches, in order to get informations on the atmospheric versus riverine contributions to sedimentation on the southern side of central Mediterranean since the last glacial. The eolian supply is dominant over the whole interval, excepted during the sapropel S1 when riverine contribution apparently became significant, and particles provenance has been modified since Last Glacial. Saharan contribution increased during the Bølling-Allerød, evidencing the persistence of aridity over North Africa although the northern Mediterranean already experienced moister and warmer conditions. The Younger Dryas is marked by proximal dust inputs highlighting intense regional eolian activity. A southward migration of dust provenance toward Sahel occurred at the onset of the Holocene, likely resulting from a southward position of the Inter Tropical Convergence Zone, probably associated with a large-scale atmospheric reorganization. Finally, a peculiar high terrigenous flux associated with drastic modifications of the mineralogical and geochemical sediment signature occurred during the sapropel S1, suggesting the propagation of fine-particles derived from major floodings of the Nile River – resulting from enhanced rainfall on northeastern Africa – and their transportation across the Sicilian-Tunisian Strait by intermediate water-masses.

20 1 Introduction

The Mediterranean is a transitional area where northern and southern climatic influences tightly interact (e.g. Magny et al., 2009). Previous studies revealed that moist conditions developed in the Mediterranean during the early Holocene while a progressive orbitally-driven trend to aridification characterized the mid and late Holocene. This climatic evolution displays a contrasting regional pattern, with an abrupt transition at 25 5.7 kyr on the western Mediterranean and a more gradual transition in the eastern

Atmospheric supply

V. Bout-Roumazeilles et al.

[Title Page](#)

[Abstract](#)

[Introduction](#)

[Conclusions](#)

[References](#)

[Tables](#)

[Figures](#)

◀

▶

◀

▶

[Back](#)

[Close](#)

[Full Screen / Esc](#)

[Printer-friendly Version](#)

[Interactive Discussion](#)



Mediterranean (Cheddadi et al., 1991; Ariztegui et al., 2000; Magny et al., 2002, 2007a; Frigola et al., 2007; Tzedakis, 2007; Sadori et al., 2008; Roberts et al., 2008, 2011; Jalut et al., 2009; Peyron et al., 2011). Precipitation estimations based on lake levels, fire and pollen association, and on speleothem and isotope records, also provide evidences of contrasting seasonality across the Mediterranean during the Holocene (Magny et al., 2003, 2007, 2009; Zanchetta et al., 2007; Tzedakis, 2007; Roberts et al., 2008; Peyron et al., 2011; Vannière et al., 2011), but estimating the respective atmospheric and oceanic control on Mediterranean climatic evolution through their impact on eolian and fluvioatile systems is still complex. A multiproxy study of the terrigenous supply would help retracing the variability of both eolian and fluvioatile systems.

The nature and provenance of fine-grained terrigenous particles in the Mediterranean is mainly controlled by the balance between riverine supplies driven by precipitation regime on the surrounding continents and eolian supplies from the Sahara (Bergametti et al., 1989b; Matthewson et al., 1995; Guerzoni and Chester, 1996; Foucault and Mélières, 2000; Goudie and Middleton, 2001). Several studies used deep-sea clay mineral associations as tracers of source regions and as indicators of water mass fluctuations (Chamley, 1975; Petschick et al., 1996; Fagel et al., 1997, 2006; Gingele et al., 2001; Liu et al., 2003; Boulay et al., 2005; Colin et al., 2010). Indeed, the mineralogical nature of sediments, which depends on the petrographic characteristics of their source areas (e.g., Bout-Roumazeilles et al., 1999; Sionneau et al., 2008), has been used to retrace detrital particles provenance in the Mediterranean and thus to assess the respective eolian and riverine contributions to deep-sea sedimentation and provide valuable information on the sediment propagation pathways (Caquineau et al., 1998, 2002; Bout-Roumazeilles et al., 2007; Erhmann et al., 2007a; Hamann et al., 2009; Kandler et al., 2009; Formenti et al., 2011a, 2011b). The clay mineral fraction also provides information on climatic conditions, such as precipitation and runoff patterns over the adjacent continents (Chamley, 1989; Montero et al., 2009, 2010), as well as on the dynamics of river inputs (Pinsak and Murray, 1960). The geochemical signature of clays would complementary help characterizing the main sources and evidencing

Atmospheric supply

V. Bout-Roumazeilles et al.

[Title Page](#)

[Abstract](#)

[Introduction](#)

[Conclusions](#)

[References](#)

[Tables](#)

[Figures](#)

◀

▶

◀

▶

[Back](#)

[Close](#)

[Full Screen / Esc](#)

[Printer-friendly Version](#)

[Interactive Discussion](#)



Atmospheric supply

V. Bout-Roumazeilles et al.

[Title Page](#)[Abstract](#)[Introduction](#)[Conclusions](#)[References](#)[Tables](#)[Figures](#)[|◀](#)[▶|](#)[◀](#)[▶](#)[Back](#)[Close](#)[Full Screen / Esc](#)[Printer-friendly Version](#)[Interactive Discussion](#)

specific transportation patterns or transfer processes (Haug et al., 2001; Kandler et al., 2009; Formenti et al., 2011a, b). Coupling clay mineral and grain-size studies would help investigating the sedimentary transfer regime because sediment grain-size distribution, which is primarily driven by sedimentary processes, reflects transportation conditions (Ehrmann et al., 2007; Montero et al., 2009; Sionneau et al., 2010). In this frame, combining clay mineralogy with grain-size analyses and geochemical tracers would allow retracing significant variations of detrital supply in the Sicilian-Tunisian strait and inferring any major modifications of both atmospheric and oceanic terrigenous transfers patterns since the last deglaciation.

10 2 Geographical settings

2.1 Oceanic circulation

The Mediterranean Sea is a concentration basin where evaporation exceeds precipitation plus freshwater discharge. The surface Atlantic water entering from Gibraltar Strait transforms into Modified Atlantic Water (MAW) as it flows eastward (Fig. 1). The eastern Mediterranean surface water displays a counterclockwise circulation (Pickard and Emery, 1982; Pinardi and Masetti, 2000). The Levantine Intermediate Water (LIW) forms in the northwest Levantine basin (Fig. 1) through convection cells at mid-depth during winter (Lascaratos et al., 1998). The LIW flows westward in sub-surface layers (~ 150 to 600–800 m) towards the northernmost Adriatic Sea and western Mediterranean (Fig. 1) via the relatively shallow Siculo-Tunisian Strait. The dense Eastern Mediterranean Deep Water (EMDW) – formed in the Adriatic Sea (Fig. 1) and occasionally in the Aegean Sea – and Western Mediterranean Deep Water (WMDW) – formed in the Gulf of Lions – fill the deep basin (< 800 m depth) (Wüst, 1961; Pickard and Emery, 1982; Malanotte-Rizzoli and Hodt, 1988; Klein et al., 1999). The Mediterranean Intermediate Water represents up to 80 % of the Mediterranean Outflow (MOW) into the Atlantic Ocean (Bryden and Stommel, 1984). This general pattern is highly dependent

on environmental conditions including eolian activity and precipitations distribution and recent alteration of the ocean/atmosphere coupling has resulted in enhanced deep-water formation in the Aegean Sea (Malanotte-Rizzoli et al., 1999).

2.2 Present-day river supplies

- 5 At present day, a major part of detrital clays is supplied to the Mediterranean via rivers (Fig. 1), the most important being the Nile River (from 120 to $230 \times 10^6 \text{ yr}^{-1}$) discharging in the eastern Mediterranean. The Po River, discharging into the Adriatic Sea ($17 \times 10^6 \text{ yr}^{-1}$) and southeastern European rivers associated with Turkish rivers, providing about respectively $30 \times 10^6 \text{ yr}^{-1}$ and $17 \times 10^6 \text{ yr}^{-1}$ to the Aegean Sea, are some
10 major contributors to sedimentation into the central Mediterranean (Holeman, 1968; Milliman and Syvitski, 1992; Stanley et al., 1992; Erhmann et al., 2007b; Garzanti et al., 2006; Hamann et al., 2009). The detrital supply through the Dardanelles Strait is reduced ($0.9 \times 10^6 \text{ yr}^{-1}$) because most sediment is trapped within the Black Sea and Marmara Sea (Erhmann et al., 2007a). Central Mediterranean is not affected by detrital supply from the Rhône River nor from the Ebro River which discharge into the
15 western Mediterranean. Finally riverine contribution to the central Mediterranean from areas bordering the southern shores is negligible due to the narrow drainage basin and sparse rainfall (Martin and Milliman, 1997).

2.3 Eolian supply

- 20 The estimation of the present-day eolian contribution to deep-sea sedimentation varies from $3.9 \times 10^6 \text{ yr}^{-1}$ to $120 \times 10^6 \text{ yr}^{-1}$ (Bergametti et al., 1989c; Matthewson et al., 1995; Guernozi and Chester, 1996; Goudie and Middleton, 2001). This wide range of estimation reflects intermittent and seasonal variations of dust outbreaks toward Europe (D'Almedia, 1986; Guerzoni et al., 1997). Satellite imagery, back trajectories
25 and observations indicate that fine particles originating from North Africa (Fig. 1) are transported by southerly/southwesterly winds (Scirocco, Ghibbli) toward the central

Atmospheric supply

V. Bout-Roumazeilles et al.

[Title Page](#)

[Abstract](#)

[Introduction](#)

[Conclusions](#)

[References](#)

[Tables](#)

[Figures](#)

[◀](#)

[▶](#)

[◀](#)

[▶](#)

[Back](#)

[Close](#)

[Full Screen / Esc](#)

[Printer-friendly Version](#)

[Interactive Discussion](#)



Atmospheric supply

V. Bout-Roumazeilles et al.

[Title Page](#)[Abstract](#)[Introduction](#)[Conclusions](#)[References](#)[Tables](#)[Figures](#)[|◀](#)[▶|](#)[◀](#)[▶](#)[Back](#)[Close](#)[Full Screen / Esc](#)[Printer-friendly Version](#)[Interactive Discussion](#)

Mediterranean (Ganor et al., 2000; Goudie and Middleton, 2001; Washington et al., 2005; Engelstaeder et al., 2006; Israelevich et al., 2012). Arid and semi-arid regions of North Africa (Fig. 1) are the main areas of production of dust all-year long (Coudé-Gaussen, 1982; Pye, 1987): Tunisia and northern Algeria, Morocco and western Sahara, the South Algeria-Mali region, the Bodélé depression and the southern Egypt-northern Sudan (Brooks and Legrand, 2000; Caquineau et al., 2002; Israelevich et al., 2002; Prospero et al., 2002; Goudie, 2003; Formenti et al., 2011a).

Most of the northward aerosols transportation across the Mediterranean is linked to the seasonal displacement of cyclones over the Mediterranean (Folger, 1970; Guerzoni et al., 1997; Moulin et al., 1997; Rodriguez et al., 2001). Maximum aerosol is observed over central and eastern Mediterranean in spring (Luck and Ben Othman, 2002; O'Hara et al., 2006) and summer when anticyclonic conditions initiates drought over the area (Prospero et al., 2002; Koren et al., 2006; Roberts, 2008; Israelevich et al., 2012). Although Saharan fine particles are mainly produced during warm and hydrolysis period, it is transported from paleosols and little consolidated formations during dry intervals when vegetation is reduced and eolian erosion more efficient (Brooks and Legrand, 2000). During summer, the Saharan depression favors the transport of dust over the western basin, progressively moving toward central Mediterranean (toward Corsica and Italy) at the end of summer (Bergametti et al., 1989a; Moulin et al., 1997; Barry and Chorley, 1998).

3 Materials and methods

3.1 Materials

The core MD04-2797CQ ($36^{\circ}57'N$ - $11^{\circ}40'E$) was taken during the PRIVILEGE-PRIMAROSA cruise in 2004 at 771 m water-depth in the Sicilian-Tunisian Strait (Fig. 1).

According to its geographical setting, the sedimentation of the core is likely influenced by both marine and eolian supplies. The scarcity of rivers along the North African

Atmospheric supply

V. Bout-Roumazeilles et al.

[Title Page](#)[Abstract](#)[Introduction](#)[Conclusions](#)[References](#)[Tables](#)[Figures](#)[|◀](#)[▶|](#)[◀](#)[▶](#)[Back](#)[Close](#)[Full Screen / Esc](#)[Printer-friendly Version](#)[Interactive Discussion](#)

margin, and their non-permanent characters prevents the area from any major and perennial fluviatile contribution (O'Hara et al., 2006). By contrast, the area is submitted to intense wind-driven supply all year long, carrying along with the dominant south-southwestern low-altitudes dusty winds (Scirocco) (Barry and Chorley, 1998) which

5 reach the Adriatic Sea by crossing the Mediterranean (Fig. 1). According to the main wind system, the proximal source of dust for the Sicilian-Tunisian strait is likely the Tunisia-northern Algeria area (Coudé-Gaussen, 1987). The Mali-Algeria frontier or the Moroccan Atlas (Brooks and Legrand, 2000; Caquineau et al., 2002; Prospero et al., 2002; Goudie, 2003) could also contribute to sedimentation either during intense dust
10 episode or when specific and/or seasonal atmospheric configuration affect the main wind directions (Bergametti et al., 1989a, 1989b; Ganor et al., 1991; Pye, 1992; Avila et al., 1997; Goudie and Middleton, 2001; Prospero et al., 2002; Washington et al., 2005).

3.2 Chronostratigraphy

15 The age model is based on 13 AMS 14C datations (Rouis-Zargouni et al., 2010, 2012). The ages were corrected using reservoir ages of 400 yr during the Holocene, the Younger Dryas and the late glacial, 560 yr during the Bølling-Allerød and 800 yr during the Heinrich event 1 and Older Dryas (H1-OD), following recommendations of Siani et al. (2001) (Table 1). The top of the core is dated at 668 ka cal. BP, suggesting that
20 the sea-sediment interface was not preserved during coring. The Terrigenous Mass Accumulation rates (MART) were calculated as follow: MART ($\text{g kyr}^{-1} \text{cm}^{-2}$) = Linear Sedimentation Rates (cm kyr^{-1}) · dry density (g cm^{-3}) · (100-(%opal + %CaCO₃)).

3.3 Clay minerals

The analyses were performed according to the protocol described in Bout-Roumazeilles et al. (1999). All samples were first decalcified with 0.2 N hydrochloric acid. The excess acid was removed by repeated centrifugations. The clay-sized fraction
25

($< 2 \mu\text{m}$) was isolated by settling, and oriented on glass slides (oriented mounts). Three XRD (X-ray diffraction) determinations were performed using a Bruker D4 Endeavor coupled with Lynxeye detector: (a) untreated sample; (b) glycolated sample (after saturation for 12 h in ethylene glycol); (c) sample heated at 490°C for two hours. Each clay mineral is then characterized by its layer plus interlayer interval as revealed by XRD analysis. Smectite is characterized by a peak at 14 \AA on the untreated sample test, which expands to 17 \AA after saturation in ethylene glycol and retracts to 10 \AA after heating. Illite presents a basal peak at 10 \AA on the three tests (natural, glycolated, and heated). The illite crystallinity, or Kübler Index is based on the expression of the width of the illite peak at 10 \AA and allows identifying the anchizone, the limit of diagenesis and the onset of the epizone. Chlorite is characterized by peaks at 14 \AA , 7 \AA , 4.72 \AA and 3.53 \AA on the three tests. Kaolinite is characterized by peaks at 7 \AA and 3.57 \AA on the untreated sample and after saturation in ethylene glycol. Both peaks disappear or are strongly reduced after heating. Palygorskite presents a basal peak at 10.34 \AA , accompanied by a weaker peak at 6.44 \AA , on both untreated and glycolated tests. The 10.34 \AA peak collapses at 10 \AA after heating (Brindley and Brown, 1980). The presence of palygorskite has been confirmed by MET observations of the palygorskite-rich samples. Semi-quantitative estimation of clay mineral abundances, based on the pseudo-voigt deconvolution for the doublets illite-palygorskite (10 \AA – 10.34 \AA) and kaolinite-chlorite (3.57 \AA – 3.53 \AA), was performed using the software MacDiff developed by Petschick (2001).

3.4 Grain-size

Grain-size analyses were performed on the carbonate- and opal-free fraction of the sediment using a Malvern Mastersizer 2000 laser (0.02 – $2000 \mu\text{m}$) following protocols described in details in Montero et al. (2009). After deflocculation, an aliquot of the sample was measured using 10 % ultrasonication in the Hydro S dispersion cell, once beam obscuration ranges between 12 and 15 %. The mode (i.e. most frequent grain-size in

Atmospheric supply

V. Bout-Roumazeilles et al.

[Title Page](#)[Abstract](#)[Introduction](#)[Conclusions](#)[References](#)[Tables](#)[Figures](#)[|◀](#)[▶|](#)[◀](#)[▶](#)[Back](#)[Close](#)[Full Screen / Esc](#)[Printer-friendly Version](#)[Interactive Discussion](#)

μm), the percentage of clay (< 2 μm), cohesive silt (2–10 μm), sortable-silt (10–63 μm) and sand (> 63 μm) are reported.

3.5 XRF-scanning

Elemental abundances were measured on U-channels using the Avaatech core scanner from the EPOC laboratory at the University of Bordeaux. The sediment was protected with Ultralene® X-ray transmission foil in order to avoid contamination. The data were acquired at a 30 s count time, using 10 kV voltage and 400 mA intensity. The results are expressed in counts per second, with a 2 % precision according to standard samples. Trace elements are normalized to Al (Tribouillard et al., 2008), in order to avoid dilution effect by carbonates.

4 Results

4.1 Clay mineralogy

The clay mineral fraction is composed of kaolinite (45 %), smectite (25 %) and illite (15 %). Chlorite and palygorskite are secondary components with 10 and 6 % of the clay content respectively (Table S1). The composition of the clay mineral assemblage displays some variations over the studied interval (Fig. 2). The kaolinite content remains slightly below 45 % between 18.5 and 11.7 ka. After what it increases and represents 50 % between 10.5 and 8.5 ka. The percentage of kaolinite decreases at 8.5 ka and remains low between 8 and 5.8 ka. It then increases progressively between 5.8 and 2 ka and reached its maximum (> 50 %) around 2 ka. The smectite remains stable between 18.5 and 8.5 ka excepted two maxima around 12 ka and 11 ka (Fig. 2). The content in smectite increases up to 38 % of the clay mineral fraction between 8.5 and 5.8 ka as the kaolinite content is minimum. This smectite-rich interval is interrupted by a slightly depleted level around 7.2 ka (Fig. 2). The smectite content decreases progressively since 5.8 ka down to 15 % at the top of the core. The illite content is maximum

[Title Page](#)

[Abstract](#)

[Introduction](#)

[Conclusions](#)

[References](#)

[Tables](#)

[Figures](#)

◀

▶

◀

▶

[Back](#)

[Close](#)

[Full Screen / Esc](#)

[Printer-friendly Version](#)

[Interactive Discussion](#)



between 18.5 and 11.7 ka, then it drops down and remains low (< 15 %) between 11.7 and 5 ka. Then illite increases slightly and remains stable around 15 % over the more recent part of the record (Fig. 2). The Kübler Index is low (< $0.4^{\circ}2\theta$) indicating high structural order when the content in illite is maximum. By contrast, the Kübler Index is higher (< $0.5^{\circ}2\theta$) – low ordering- between 11.7 and 5 ka when the percentage of illite is reduced. The illite to kaolinite ratio (I/K) is characterized by a drastic change at 11.7 ka from values around 0.35 to values as low as 0.25. The chlorite content does not correlate with other clay species and shows slight variations, being higher than average between 18.5 and 15.5 ka. The palygorskite is less abundant between 8.5 and 5.8 ka, while smectite is maximum (Fig. 2).

4.2 Grain-size

The grain-size varies between 4 μm and 10 μm , indicating the detrital fraction is mainly composed of cohesive silt-size particles. Cohesive particles indeed represent 50 to 70 % of the total terrigenous fraction, being slightly less abundant between 18.5 and 11.7 ka and between 7.5 and 5.5 ka (Fig. 3). By contrast, the clay-size fraction is generally low (around 11 %), excepted between 8.5 and 5.5 ka when it represents up to 25 % of the detrital material. The sortable silt (10 μm to 63 μm) composes 25 % of the detrital fraction, being more abundant between 13 and 12 ka where it represents 45 %. The sand-size fraction is rare, but shows two maxima between 14 and 12 ka and between 8.5 and 7.5 ka (Fig. 3).

4.3 Elemental geochemistry

The Al content displays a decreasing trend from 18.5 to 14 ka (Fig. 4). The Ca to Fe ratio is used to distinguish areas dominated by carbonates (Sahara) from areas where hydrolysis is intense (alterites). The Ca/Fe ratio is characterized by large variations, with maximum values between 15 and 13 ka, and between 5 and 3 ka, while the ratio is minimum before 15 ka and between 2 and 1 ka. Some intervals are characterized

8, 2921–2968, 2012

CPD

Atmospheric supply

V. Bout-Roumazeilles et al.

Title Page

Abstract

Introduction

Conclusions

References

Tables

Figures

◀

▶

◀

▶

Back

Close

Full Screen / Esc

Printer-friendly Version

Interactive Discussion



by higher than average K/Al ratio, between 14 and 11.7, between 5.8 and 5.5 ka and between 2.5 and 1 ka. The two latter intervals are also characterized by the highest values of the Ti/Al ration (Fig. 4). The Zr/Al ratio displays a peculiar behavior, peaking at 13.4 ka, 7 ka, 6.4 ka, 1.3 ka and being high between 12.8 and 12.3 ka.

CPD

8, 2921–2968, 2012

5 Discussion

5.1 Mineralogical and geochemical characterization of particle provenance and transport patterns

Illite and chlorite are abundant in sediments from the Ionian Sea (Fig. 1), where they mainly derive from the southern European rivers flowing into the Adriatic (Po River)

and Aegean Seas (southeastern European Rivers) (Venkatarathnam and Ryan, 1971; Dominik and Stoffers, 1978; Chamley, 1989; Alonso and Maldonado, 1990; Tomadin, 2000). Smectite predominates in the eastern basin, being abundant in the Marmara Sea (Ergin et al., 2012; Armynot et al., 2012), in the Levantine basin (Hamann et al., 2009) and in the southeastern Aegean Sea (Erhmann et al., 2007a). Smectite char-

acterizes the Nile River suspended loads, deriving from Cenozoic volcanic provinces of the Ethiopian Highlands (Ukstins et al., 2002; Hamann et al., 2009), and is further redistributed as suspended clay particles within the Mediterranean surface wa-

ter (Venkatarathnam and Ryan, 1971; Foucault and Mélières, 2000; Hamann et al., 2009). Palygorskite has been shown to be abundant in tunisian dunes and is used as a main eolian tracer, because it may be transported over long-range distance, crossing the Mediterranean through meridian transfers (Coudé-Gaussen et al., 1982; Robert et al., 1984; Molinaroli, 1996). Illite is also a dominant component of eolian dust orig-

inating from Sahara when associated with palygorskite (Coudé-Gaussen and Blanc, 1985; Guerzoni et al., 1999; Foucault and Mélières, 2000; Goudie and Middleton, 2001), whereas illite associated with abundant kaolinite originate from southeastern areas of North Africa (Chester et al., 1977; Stanley and Wingerath, 1996; Foucault

Atmospheric supply

V. Bout-Roumazeilles et al.

[Title Page](#)

[Abstract](#)

[Introduction](#)

[Conclusions](#)

[References](#)

[Tables](#)

[Figures](#)

[◀](#)

[▶](#)

[◀](#)

[▶](#)

[Back](#)

[Close](#)

[Full Screen / Esc](#)

[Printer-friendly Version](#)

[Interactive Discussion](#)



Atmospheric supply

V. Bout-Roumazeilles et al.

[Title Page](#)[Abstract](#)[Introduction](#)[Conclusions](#)[References](#)[Tables](#)[Figures](#)[|◀](#)[▶|](#)[◀](#)[▶](#)[Back](#)[Close](#)[Full Screen / Esc](#)[Printer-friendly Version](#)[Interactive Discussion](#)

The grain-size of dust displays strong seasonal variations (Guerzoni et al., 1997), with a fine population (2 to 10 µm, mode around 2.7 µm) characterizing long-distance and high latitude transport and a coarser population (5 to 50 µm, mode around 20 µm) typical of dust storms carried over few km, being restricted to adjacent continental and

5 marine areas (Prospero, 1981; Torres-Padron et al., 2002). Comparison between Ti/Al and Zr/Al ratios and grain-size distribution are thus used to identify specific eolian vs. riverine transport processes, associated with the development of sand dunes during the Holocene, or with remote fine-grained eolian outbreaks or coarse-grained fluvial supply (Haug et al., 2001; Martinez-Ruiz et al., 2003; Erhmann et al., 2007b; Hamann
10 et al., 2009; Montero et al., 2009; Skonieczny et al., 2011).

5.2 Bølling-Allerød

The Bølling-Allerød (B-A) is marked by enhanced terrigenous supply starting at 14.6 ka, associated with increased contributions of both illite and palygorskite while kaolinite and chlorite decrease (Fig. 2). The relationship between illite content and sortable silt-size fraction (14 µm) indicate that illite is mostly transported through eolian processes. The concomitant increase of the Ca/Fe and I/K ratio suggests that the increased eolian supply is associated with a modification of the main detrital source (Fig. 5a). Indeed, increased proportion of Ca vs. Fe during the B-A may basically be interpreted as reflecting higher productivity but this hypothesis is not supported by the dinoflagellite record from core MD04-2797 (Rouis-Zargouni et al., 2010). The increased proportion of illite may indicate a northward migration of the main clay provenance over Libya, as illite has been shown to be more abundant in dust collected over northern Libya (O'Hara et al., 2006). Nevertheless the I/K ratio range – varying between 0.35 and 0.4 – during the B-A is rather low compared with observed values for Libya and does not further support this hypothesis (Fig. 5a). The observed sedimentological characteristics tend to indicate Tunisia-Algeria as the main dust provenance (Formenti et al., 2011a). According to previously published data, the mineralogical composition is indeed consistent with a source from northern or central Algeria (Fig. 7a), but the low content in

CPD

8, 2921–2968, 2012

Atmospheric supply

V. Bout-Roumazeilles et al.

[Title Page](#)

[Abstract](#)

[Introduction](#)

[Conclusions](#)

[References](#)

[Tables](#)

[Figures](#)

◀

▶

◀

▶

[Back](#)

[Close](#)

[Full Screen / Esc](#)

[Printer-friendly Version](#)

[Interactive Discussion](#)



palygorskite ruled out any major contribution from tunisian loess (Bout-Roumazeilles et al., 2007). The development of humid conditions during the B-A is evidenced by an increased contribution of river vs. eolian supply in the Aegean Sea (core SL128, Fig. 1) (Hamann et al., 2008), by pollen association from the Alboran (ODP976, Fig. 1) and Adriatic Sea (Combourieu-Nebout et al., 1998, 2002; Fletcher and Sanchez-Goñi, 2008) and by a speleothem record from the eastern Mediterranean (Bar-Matthew et al., 2003), contrasting with the clay mineral record from the Sicilian-Tunisian Strait. The Sea Surface Temperatures (SST, Fig. 3) – as reconstructed from planktonic *foraminifera* at site MD04-2797 – are high during the Bølling-Allerød (Ellassami et al., 2007), consistently with general warm oceanic conditions, relatively high humidity and temperatures compared with present-day in Sicily and central Mediterranean (Ramrath et al., 2000; Allen et al., 2002; Zielhofer et al., 2008; Incarbona et al., 2010). The dominance of semi-desert plants at site MD04-2797 (Desprat et al., 2012) confirms the persistence of dry continental conditions over Africa during the B-A. These results tend to confirm contrasting climatic evolution (e.g. Roberts et al., 2008) with humid conditions on the northeastern and eastern Mediterranean whereas aridity still persisted on the southern Mediterranean.

5.3 Younger Dryas

A major peak in the Zr/Al ratio is observed between around 12.8 ka, associated with an increase in the abundance of both sortable-silt and sand-size particles (Fig. 5b). The clay association does not exhibit major modification but smectite is more abundant at the expense of kaolinite, displaying a peak at 12 ka (Fig. 2). These characteristics indicate the supply of coarser particles that may either be associated to a volcanic supply, or to river supply or to an intense dust episode (Martinez-Ruiz et al., 2003; Erhmann et al., 2007b; Hamann et al., 2009; Skonieczny et al., 2011). Smectite peaking at 12 ka supports the hypothesis of a tephra (Fig. 5d). Moreover, when compared with the chronology of tephras (e.g. Zanchetta et al., 2011), the increase of Zr may be associated with the Agrano Pomici Principali (12.8–12.2 ka) tephra (DiVito et al.,

[Title Page](#)[Abstract](#)[Introduction](#)[Conclusions](#)[References](#)[Tables](#)[Figures](#)[|◀](#)[▶|](#)[◀](#)[▶](#)[Back](#)[Close](#)[Full Screen / Esc](#)[Printer-friendly Version](#)[Interactive Discussion](#)

Atmospheric supply

V. Bout-Roumazeilles et al.

[Title Page](#)[Abstract](#)[Introduction](#)[Conclusions](#)[References](#)[Tables](#)[Figures](#)[|◀](#)[▶|](#)[◀](#)[▶](#)[Back](#)[Close](#)[Full Screen / Esc](#)[Printer-friendly Version](#)[Interactive Discussion](#)

Grousset et al., 1992; Crouvi et al., 2010) and further supported by model suggesting that Libyan desert and coastal areas are major coarse-grain dust sources for central and eastern Mediterranean (Callot et al., 2000), may thus reflect local eolian activity forced by ocean-atmosphere linkage at global scale (Fig. 7b).

5 5.4 Onset of the Holocene

The end of the Younger Dryas (11.7 ka) is marked by a drastic change in the clay assemblage (Figs. 5a, 6a and b) and a decrease of the sortable silt proportion. The kaolinite increases while illite diminishes, resulting in a progressive decrease of the I/K ratio. This shift, associated to a modification of the illite structural composition, 10 evidences a major change of provenance of the clay fraction, interpreted as an increase contribution of the Sahelian area (Fig. 6a). This observation is supported by the synchronous changes in geochemical signature (Fig. 6c) confirming enhanced contribution of strongly hydrolyzed domains. Low I/K indicates enhanced contribution from the southern Algeria-Mali border region (Paquet et al., 1984; Bergametti et al., 1989b; 15 Alastuey et al., 2005; Bout-Roumazeilles et al., 2007), but the clay association suggests a provenance from southern Algeria rather than from northern Mali, because kaolinite is more abundant southward (e.g. Bout-Roumazeilles et al., 2007), becoming dominant in southern Algeria whereas the Mali border is characterized by smectite-rich assemblages (Fig. 7c). The abundance of semi-desert pollen taxa exhibits a sharp decrease at 12.25 ka (Desprat et al., 2012), before the mineralogical transition, suggesting 20 that the modification of vegetation, i.e. a major change in steppe composition and a development of scarce deciduous oak woodlands, might prevent soils from weathering, displacing southward the areas of eolian erosion. The end of the YD is marked by a similar modification of the clay mineral fraction in a core from the northeastern 25 Tropical Atlantic off Senegal (Skonieczny et al., 2012) and interpreted as recording a southward shift of the Inter Tropical Convergence Zone (ITCZ), which strongly affect the transport of Saharan dust toward the Atlantic Ocean. Moreover, the onset of the Holocene is also marked by a decrease of the I/K ratio off Portugal (Stumpf et al.,

CPD

8, 2921–2968, 2012

Atmospheric supply

V. Bout-Roumazeilles et al.

[Title Page](#)

[Abstract](#)

[Introduction](#)

[Conclusions](#)

[References](#)

[Tables](#)

[Figures](#)

◀

▶

◀

▶

[Back](#)

[Close](#)

[Full Screen / Esc](#)

[Printer-friendly Version](#)

[Interactive Discussion](#)



Atmospheric supply

V. Bout-Roumazeilles et al.

[Title Page](#)[Abstract](#)[Introduction](#)[Conclusions](#)[References](#)[Tables](#)[Figures](#)[◀](#)[▶](#)[◀](#)[▶](#)[Back](#)[Close](#)[Full Screen / Esc](#)[Printer-friendly Version](#)[Interactive Discussion](#)

2011). The synchronicity of the clay modification at these sites, submitted to distinct wind regimes, signify that the end of the YD is marked by a large-scale atmospheric re-organization over the North African continent, with the development of dry conditions during the early Holocene, affecting both the high-latitude long-range transportation and the regional low-latitude wind regime over the Mediterranean.

5.5 Sapropel S1

The time interval between 8.6 and 5.5 ka is marked by the highest terrigenous flux and smectite content, with a significant grain-size fining (Figs. 2 and 5d). The associated increase in particulate organic carbon (POC) during the whole interval suggests presapropellic conditions (Essallami et al., 2007). Both timing and peculiar characteristics suggest this interval to be related to the most recent organic-rich sapropel S1 (Kidd et al., 1978) deposited during the mid-Holocene in the eastern Mediterranean (Emeis et al., 1996; Emeis et al., 2000; De Lange et al., 2008). During the sapropel, increased precipitation on the surrounding continents provided freshwater discharge and promoted strong stratification of the water column and enhanced nutrient supply, resulting in increased productivity and improved preservation due to oxygen depletion of the water column (Rossignol-Strick et al., 1982; Rohling, 1994; Abu-Zied et al., 2008). Increased precipitations are thought to be linked to either orbitally-forced enhanced monsoon activity (Rossignol-Strick et al., 1982; Hilgen, 1991; Lourens et al., 1996; Emeis et al., 2000) or to increased rainfall over the Mediterranean region (Kallel et al., 1997; Magny et al., 2002). Indeed, although some data appear to be consistent over the Mediterranean basin (Saduri et al., 2011), rainfall records display seasonal modulation (Saduri et al., 2004, 2008; Frisia et al., 2006; Magny et al., 2007, 2012; Kotthoff et al., 2008; Jalut et al., 2009; Colonese et al., 2010; Giraudi et al., 2011; Peyron et al., 2011). Speleothems indicate increased moisture availability in both western (Corchia Cave, Zanchetta et al., 2007), and eastern Mediterranean (Soreq Cave, Bar-Matthews et al., 2000) consistent with lakes records from East Anatolia (Stevens et al., 2001; e.g. Roberts et al., 2008) but also evidence contrasting moisture originating either from

the Atlantic (Bard et al., 2002) or from the Mediterranean (Arz et al., 2003). Moreover rainfall patterns also display slightly different chronology in Italian lakes (Roberts et al., 2008) and stalagmite records (Frisia et al., 2006; Zanchetta et al., 2007). Consequently, most studies focused on the precipitation distribution and moisture availability that prevailed on the continent at the time of S1.

But investigations of the marine propagation of the sapropelic layer from eastern toward western Mediterranean evidenced the absence of true sapropels and/or synchronous events (Mercone et al., 2000) in the western basin, suggesting lower export of production fluxes into the basin (Martinez-Ruiz et al., 2003) or different hydrographic conditions (Weldeab et al., 2003). Smectite provenance during the sapropel in the Sicilian-Tunisian Strait would provide additional information on the modifications of oceanic environmental conditions. Indeed, central Mediterranean is depleted in smectite (Bout-Roumazeilles et al., 2007), which is rare in southern Algeria and absent from northern and central Algeria. By contrast, the southern Algeria-Mali border (Fig. 1) is locally characterized by a high content in smectite (Bout-Roumazeilles et al., 2007). But, at present-day, this area is submitted to trade-winds, promoting a dominant low-altitude westward transportation and ruling out any significant contribution of this area to sedimentation in the central Mediterranean. A volcanic origin of smectite from Sicilia is not supported by optical observations or by the chronology of the main tephra (Siani et al., 2004). The enhanced supply of smectite may originate from tunisian loess (Fig. 1) (e.g. Bout-Roumazeilles et al., 2007), but the low content of palygorskite during the smectite-rich interval does not further support this interpretation. Moreover, the enhanced moisture availability over that period, associated with pollen association – i.e. open oak forest with heath underbrush or maquis and Asteraceæ-Poaceæ-Cyperaceæ steppe (Desprat et al., 2012) preventing soils from erosion – and the geochemical signal give little support to significant eolian activity. These observations highlight that smectite may alternatively be supplied toward the Mediterranean by the Nile River and transported as suspended particles within the Mediterranean surface water (Ventakatarathnam and Ryan, 1971; Stanley and Wingerath, 1996; Foucault

Atmospheric supply

V. Bout-Roumazeilles et al.

[Title Page](#)

[Abstract](#)

[Introduction](#)

[Conclusions](#)

[References](#)

[Tables](#)

[Figures](#)

[|◀](#)

[▶|](#)

[◀](#)

[▶](#)

[Back](#)

[Close](#)

[Full Screen / Esc](#)

[Printer-friendly Version](#)

[Interactive Discussion](#)



Atmospheric supply

V. Bout-Roumazeilles et al.

[Title Page](#)[Abstract](#)[Introduction](#)[Conclusions](#)[References](#)[Tables](#)[Figures](#)[|◀](#)[▶|](#)[◀](#)[▶](#)[Back](#)[Close](#)[Full Screen / Esc](#)[Printer-friendly Version](#)[Interactive Discussion](#)

5.6 Late Holocene

Atmospheric supply

V. Bout-Roumazeilles et al.

[Title Page](#)

[Abstract](#)

[Introduction](#)

[Conclusions](#)

[References](#)

[Tables](#)

[Figures](#)

[◀](#)

[▶](#)

[◀](#)

[▶](#)

[Back](#)

[Close](#)

[Full Screen / Esc](#)

[Printer-friendly Version](#)

[Interactive Discussion](#)



6 Conclusions

The clay mineral, grain-size and geochemical studies of sediment deposited on the Sicilian-Tunisian Strait help retracing atmospheric vs. riverine terrigenous supplies variability since the last glacial in central Mediterranean. Although the eolian supply is dominant at the studied site – excepted during the sapropel S1 – both flux and the main provenance of particles display strong variations, related to aridity/moisture balance and vegetation cover, driven by large-scale atmospheric reorganization.

The Bølling-Allerød is marked by increased terrigenous flux while both illite and palygorskite became main components of the clay mineral fraction. The concomitant dominance of silt-size particles indicates an eolian origin for this enhanced detrital supply. The geochemical and mineralogical data indicate a dominant Saharan contribution, pinpointing central and northern Algeria as a main provenance. This increased eolian contribution from Sahara highlights contrasting regional climatic evolution, with the development of moist conditions over the North and eastern Mediterranean during the Bølling-Allerød, while glacial aridity persisted on the southern Mediterranean.

A short-term coarse-grained and Zr-rich interval characterized the Younger Dryas, as arid and cold climatic conditions promoted soil erosion. Similar events characterize the western Mediterranean and the northeastern Tropical Atlantic Ocean, although clay mineralogy clearly indicates different provenances. These results suggest local increase of wind activity driven by wide ocean-atmosphere interactions.

The onset of the Holocene is marked by a major change of clay mineralogy and crystallinity corresponding to a southward migration of the main clay provenance toward the Sahelian belt. This change is associated with a progressive development of the Mediterranean vegetation and the southward shift of the ITCZ. Similar signals are recorded in the northeastern tropical Atlantic Ocean and off Portugal, suggesting a large-scale atmospheric reorganization.

High terrigenous flux associated with the dominance of very fine-grained Pd-rich smectite characterized the early to mid-Holocene in central Mediterranean, while the

CPD

8, 2921–2968, 2012

Atmospheric supply

V. Bout-Roumazeilles et al.

[Title Page](#)

[Abstract](#)

[Introduction](#)

[Conclusions](#)

[References](#)

[Tables](#)

[Figures](#)

◀

▶

◀

▶

[Back](#)

[Close](#)

[Full Screen / Esc](#)

[Printer-friendly Version](#)

[Interactive Discussion](#)



organic content indicates pre-sapropelic conditions. The sedimentological characteristics rule out any eolian supply but rather suggest enhanced riverine contribution from remote area during the sapropel S1. The peculiar signature of this event in the central Mediterranean and in the Levantine basin suggests the propagation through intermediate water-masses of fine-grained smectite originating from the Nile River during the sapropel S1, resulting from enhanced precipitations on northeast Africa, coincident with the late phase of the AHP.

Finally, an increase supply of dust originating from northern Sahel or southern Morocco characterizes the last 3 kyr, indicating intense eolian activity linked to modification of the rainfall regime.

**Supplementary material related to this article is available online at:
<http://www.clim-past-discuss.net/8/2921/2012/cpd-8-2921-2012-supplement.pdf>.**

Acknowledgements. This study was funded by the ANR LAMA. Philippe Martinez (EPOC – University of Bordeaux) is thanked for producing XRF analysis of the core. Léa-Marie Bernard Emaille, Deny Malengros and Romain Abraham are thanked for technical assistance for XRD analysis and laser grain-size measurements.



²⁰ The publication of this article is financed by CNRS-INSU.



References

- Abu-Zied, R. H., Rohling, E. J., Jorissen, F. J., Fontanier, C., Casford, J. S. L., and Cooke, S.: Benthic *foraminiferal* response to changes in bottom-water oxygenation and organic carbon flux in the eastern Mediterranean during LGM to Recent times, *Mar. Micropaleontol.*, 67, 46–68, 2008.
- Alastuey, A., Querol, X., Castillo, S., Escudero, M., Avila, A., Cuevas, E., Torres, C., Romero, P.-M., Exposito, F., Garcia, O., Pedro Diaz, J., Dingenen, R. V., and Putaud, J. P.: Characterization of TSP and PM2.5 at Izana and Sta. Cruz de Tenerife (Canary Islands, Spain) during a Saharan Dust Episode (July 2002), *Atmos. Environ.*, 39, 4715–4728, 2005.
- Allen, J. R. M., Watts, W. A., McGee, E., and Huntley, B.: Holocene environmental variability – The record from Lago Grande di Monticchio, Italy, *Quaternary Int.*, 88, 69–80, 2002.
- Alonso, B. and Maldonado, A.: Late Quaternary sedimentation patterns of the Ebro turbidite systems (northwestern Mediterranean): Two styles of deep-sea deposition, *Mar. Geol.*, 95, 353–377, 1990.
- Ariztegui, D., Asioli, A., Lowe, J. J., Trincardi, F., Vigliotti, L., Tamburini, F., Chondrogianni, C., Accorsi, C. A., Bandini Mazzanti, M., Mercuri, A. M., Van Der Kaars, S., McKenzie, J. A., and Oldfield, F.: Palaeoclimate and the formation of sapropel S1: inferences from Late Quaternary lacustrine and marine sequences in the central Mediterranean region, *Paleogeogr. Palaeocl.*, 158, 215–240, 2000.
- Armynot du Châtelet, E., Bout-Roumazeilles, V., Coccioni, R., Frontalini, F., Guillot, F., Kaminski, M. A., Recourt, P., Riboulleau, A., Trentesaux, A., Tribouillard, N., and Ventalon, S.: Environmental control on shell structure and composition of agglutinated *foraminifera* in the Marmara Sea, *Mar. Geol.*, submitted, 2012.
- Arz, H. W., Lamy, F., Pätzold, J., Müller, P. J., and Prins, M.: Mediterranean moisture source for an early-Holocene humid period in the Northern Red Sea, *Science*, 300, 118–121, 2003.
- Avila, A., Queralt-Mitjans, I., and Alarcón, M.: Mineralogical composition of African dust delivered by red rains over northeastern Spain, *J. Geophys. Res.*, 102, 21977–21996, 1997.
- Bar-Matthews, M., Ayalon, A., and Kaufman, A.: Timing and hydrological conditions of Sapropel events in the eastern Mediterranean, as evident from speleothems, Soreq cave, Israel, *Chem. Geol.*, 169, 145–156, 2000.
- Bar-Matthews, M., Ayalon, A., Gilmour, M., Matthews, A., and Hawkesworth, C.J.: Sea-land oxygen isotopic relationship from planktonic *foraminifera* and speleothems in the East-

Atmospheric supply

V. Bout-Roumazeilles et al.

[Title Page](#)

[Abstract](#)

[Introduction](#)

[Conclusions](#)

[References](#)

[Tables](#)

[Figures](#)

◀

▶

◀

▶

[Back](#)

[Close](#)

[Full Screen / Esc](#)

[Printer-friendly Version](#)

[Interactive Discussion](#)



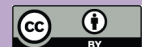
Atmospheric supply

V. Bout-Roumazeilles et al.

[Title Page](#)[Abstract](#)[Introduction](#)[Conclusions](#)[References](#)[Tables](#)[Figures](#)[|◀](#)[▶|](#)[◀](#)[▶](#)[Back](#)[Close](#)[Full Screen / Esc](#)[Printer-friendly Version](#)[Interactive Discussion](#)

Atmospheric supply

V. Bout-Roumazeilles et al.

[Title Page](#)[Abstract](#)[Introduction](#)[Conclusions](#)[References](#)[Tables](#)[Figures](#)[◀](#)[▶](#)[◀](#)[▶](#)[Back](#)[Close](#)[Full Screen / Esc](#)[Printer-friendly Version](#)[Interactive Discussion](#)

Atmospheric supply

V. Bout-Roumazeilles et al.

[Title Page](#)[Abstract](#)[Introduction](#)[Conclusions](#)[References](#)[Tables](#)[Figures](#)[|◀](#)[▶|](#)[◀](#)[▶](#)[Back](#)[Close](#)[Full Screen / Esc](#)[Printer-friendly Version](#)[Interactive Discussion](#)

Atmospheric supply

V. Bout-Roumazeilles et al.

[Title Page](#)[Abstract](#)[Introduction](#)[Conclusions](#)[References](#)[Tables](#)[Figures](#)[◀](#)[▶](#)[◀](#)[▶](#)[Back](#)[Close](#)[Full Screen / Esc](#)[Printer-friendly Version](#)[Interactive Discussion](#)

Atmospheric supply

V. Bout-Roumazeilles et al.

[Title Page](#)[Abstract](#)[Introduction](#)[Conclusions](#)[References](#)[Tables](#)[Figures](#)[|◀](#)[▶|](#)[◀](#)[▶](#)[Back](#)[Close](#)[Full Screen / Esc](#)[Printer-friendly Version](#)[Interactive Discussion](#)

Atmospheric supply

V. Bout-Roumazeilles et al.

[Title Page](#)[Abstract](#)[Introduction](#)[Conclusions](#)[References](#)[Tables](#)[Figures](#)[|◀](#)[▶|](#)[◀](#)[▶](#)[Back](#)[Close](#)[Full Screen / Esc](#)[Printer-friendly Version](#)[Interactive Discussion](#)

Atmospheric supply

V. Bout-Roumazeilles et al.

[Title Page](#)[Abstract](#)[Introduction](#)[Conclusions](#)[References](#)[Tables](#)[Figures](#)[◀](#)[▶](#)[◀](#)[▶](#)[Back](#)[Close](#)[Full Screen / Esc](#)[Printer-friendly Version](#)[Interactive Discussion](#)

Grousset, F. E., Rognon, P., Coudé-Gaussen, G., and Pédemay, P.: Origins of peri-Saharan dust deposits traced by their Nd and Sr isotopic composition, *Paleogeogr. Palaeoecol.*, 93, 203–212, 1992.

5 Guerzoni, S. and Chester, R.: The impact of Desert Dust across the Mediterranean, Dordrecht, Kluwer Academic, 1996.

Guerzoni, S., Molinaroli, E., and Chester, R.: Saharan dust inputs to the Western Mediterranean Sea: depositional patterns, geochemistry and sedimentological implications, *Deep-Sea Res. Pt. II*, 44, 631–654, 1997.

10 Guerzoni, S., Chester, R., Dulac, F., Herut, B., Loyë-Pilot, M.-D., Measures, C., Migon, C., Molinaroli, E., Moulin, C., Rossini, P., Saydam, C., Soudine, A., and Ziveri, P.: The role of atmospheric deposition in the biogeochemistry of the Mediterranean Sea, *Prog. Oceanogr.*, 44, 147–190, 1999.

15 Guieu, C., Loyë-Pilot, M. D., Ridame, C., and Thomas, C.: Chemical characterization of the Saharan dust end-member: Some biogeochemical implications for the western Mediterranean Sea, *J. Geophys. Res.*, 107, 4258, doi:10.1029/2001jd000582, 2002.

Hamann, Y., Ehrmann, W., Schmiedl, G., Krüger, S., Stuut, J.-B., and Kuhnt, T.: Sedimentation processes in the Eastern Mediterranean Sea during the Late Glacial and Holocene revealed by end-member modelling of the terrigenous fraction in marine sediments, *Mar. Geol.*, 248, 97–114, 2008.

20 Hamann, Y., Ehrmann, W., Schmiedl, G., and Kuhnt, T.: Modern and late Quaternary clay mineral distribution in the area of the SE Mediterranean Sea, *Quaternary Res.*, 71, 453–464, 2009.

25 Hamann, Y., Bowen, S. W., Ersoy, O., Ehrmann, W., and Aydar, E.: First evidence of a distal early Holocene ash layer in Eastern Mediterranean deep-sea sediments derived from the Anatolian volcanic province, *Quaternary Res.*, 73, 497–506, 2010.

Haug, G., Hughen, K. A., Sigman, D. M., Peterson, L. C., and Röhl, U.: Southward migration of the Intertropical Convergence Zone through the Holocene, *Science*, 293, 1304–1308, 2001.

30 Hilgen, H. J.: Astronomical calibration of Gauss to Matuyama sapropels in the Mediterranean and implication for the geomagnetic polaritytime scale, *Earth Planet. Sc. Lett.*, 104, 226–244, 1991.

Holeman, J. N.: The sediment yield of major rivers of the world, *Water Resour. Res.*, 4, 737–744, 1968.

- Incarbona, A., Martrat, B., Di Stefano, E., Grimalt, J. O., Pelosi, N., Patti, B., and Tranchida, G.: Primary productivity variability on the Atlantic Iberian margin over the last 70,000 years: evidence from coccolithophores and fossil organic compounds, *Paleoceanography*, 25, PA2218, doi:10.1029/2008PA001709, 2010.
- 5 Israelevich, P. L., Levin, Z., Joseph, J. H., and Ganor, E.: Desert aerosol transport in the Mediterranean region as inferred from TOMS aerosol index, *J. Geophys. Res.*, 107, 4572, doi:10.1029/2001jd002011, 2002.
- Israelevich, P., Ganor, E., Alpert, P., Kishcha, P., and Stupp, A.: Predominant transport paths of Saharan dust over the Mediterranean Sea to Europe, *J. Geophys. Res.*, 117, D02205, doi:10.1029/2011JD016482, 2012.
- 10 Jalut, G., Deboubat, J. J., Fontugne, M., and Otto, T.: Holocene circum-Mediterranean vegetation changes: climate forcing and human impact, *Quaternary Int.*, 200, 4–18, 2009.
- Jones, G. A.: Advective transport of clay minerals in the region of the Rio Grande rise, *Mar. Geol.*, 58, 187–212, 1984.
- 15 Kallel, N., Paterne, J. C., Duplessy, C., Vergnaud-Grazzini, C., Labeyrie, L., Arnold, M., Fontugne, M., and Pierre, C.: Enhanced rainfall in the Mediterranean region during the last sapropel event, *Oceanol. Acta*, 20, 697–712, 1997.
- 20 Kandler, K., Schütz, L., Deutscher, C., Ebert, M., Hofmann, H., Jäckel, S., Jaenicke, R., Knippertz, P., Lieke, K., Massling, A., Petzold, A., Schladitz, A., Weinzierl, B., Wiedensohler, A., Zorn, S., and Weinbruch, S.: Size distribution, mass concentration, chemical and mineralogical composition and derived optical parameters of the boundary layer aerosol at Tifou, Morocco, during SAMUN 2006, *Tellus B*, 61, 32–50, 2009.
- 25 Kidd, R. B., Cita, M. B., and Ryan, W. B. F.: Stratigraphy of the Eastern Mediterranean Sapropel Sequences Recovered during DSDP LEG 42A and Their Paleoenvironmental Significance, edited by: Hsü, K. J., Montadert, L., Garrison, R. E., Fabricius, F. H., Kidd, R. B., Müller, C., Cita, M. B., Bizon, G., Wright, R. C., Erickson, A. J., Bernoulli, D., and Mélières, F., *Initial Rep. Deep Sea* 42, US Govt. Printing Office, Washington, DC, 421–443, 1978.
- Kieft, L., McTainsh, G. H., and Nickling, W. G.: Sedimentological characteristics of Saharan and Australian Dusts, in: *The Impact of Desert Dust Across the Mediterranean*, edited by: Guerzoni, S. and Chester, R., Kluwer Academic Publishers, Dordrecht, 183–190, 1996.
- 30 Kim, J., Jung, C. H., Choi, B.-C., Oh, S.-N., Brechtel, F. J., Yoon, S.-C., and Kim, S.-W.: Number size distribution of atmospheric aerosols during ACE-Asia dust and precipitation events, *Atmos. Environ.*, 41, 4841–4855, 2007.

Atmospheric supply

V. Bout-Roumazeilles et al.

[Title Page](#)[Abstract](#)[Introduction](#)[Conclusions](#)[References](#)[Tables](#)[Figures](#)[◀](#)[▶](#)[◀](#)[▶](#)[Back](#)[Close](#)[Full Screen / Esc](#)[Printer-friendly Version](#)[Interactive Discussion](#)

Atmospheric supply

V. Bout-Roumazeilles et al.

[Title Page](#)[Abstract](#)[Introduction](#)[Conclusions](#)[References](#)[Tables](#)[Figures](#)[|◀](#)[▶|](#)[◀](#)[▶](#)[Back](#)[Close](#)[Full Screen / Esc](#)[Printer-friendly Version](#)[Interactive Discussion](#)

- Magny, M., Vanni  re, B., de Beaulieu, J.-L., B  geot, C., Heiri, O., Millet, L., Peyron, O., and Walter-Simonnet, A. V.: Early-Holocene climatic oscillations recorded by lake-level fluctuations in west-central Europe and in central Italy, *Quaternary Sci. Rev.*, 26, 1951–1964, 2007.
- Magny, M., Vanni  re, B., Zanchetta, G., Fouache, E., Touchais, G., Petrika, L., Coussot, C., 5 Walter-Simonnet, A. V., and Arnaud, F.: Possible complexity of the climatic event around 4300–3800 cal BP in the central and western Mediterranean, *Holocene*, 19, 823–833, 2009.
- Magny, M., Peyron, O., Sadori, L., Ortu, E., Zanchetta, G., Vanni  re, B., and Tinner, W.: Contrasting patterns of precipitation seasonality during the Holocene in the south- and north-central Mediterranean, *J. Quaternary Sci.*, 27, 290–296, 2012.
- 10 Malanotte-Rizzoli, P. and Hecht, A.: Large-scale properties of the Eastern Mediterranean: a review, *Oceanol. Acta*, 11, 323–335, 1988.
- Malanotte-Rizzoli, P., Manca, B. B., Ribera, D., Alcala, M., Theocharis, A., Brenner, S., Budillon, G., and Ozsoy, E.: The Eastern Mediterranean in the 80s and in the 90s: the big transition in the intermediate and deep circulations, *Dynam. Atmos. Oceans*, 29, 365–395, 1999.
- 15 Martin, J. M. and Milliman, J. D.: EROS 2000 (European Rivers Ocean System). The western Mediterranean Sea: an introduction, *Deep-Sea Res.*, 44, 521–529, 1997.
- Martinez-Ruiz, F., Paytan, A., Kastner, M., Gonzalez-Donoso, J. M., Linares, D., Bernasconi, S., and Jimenez-Espejo, F. J.: A comparative study of the geochemical and mineralogical characteristics of the S1 sapropel in the western and eastern Mediterranean, *Palaeogeogr. Palaeoocl.*, 190, 23–37, 2003.
- 20 Matthewson, A. P., Shimmield, G., Kroon, D., and Fallick, A. E.: A 300 kyr high-resolution aridity record of the North African continent, *Paleoceanography*, 10, 677–692, 1995.
- Mayewski, P. A., Rohling, E. J., Stager, J. C., Karlen, W., Maasch, K. A., Meeker, L. D., Meyer-25 son, E. A., Gasse, F., Van Kreveld, S., Holmgren, K., Lee-Thorp, J., Rosqvist, G., Rack, F., Staubwasser, M., Schneider, R. R., and Steig, E. J.: Holocene climate variability, *Quaternary Res.*, 62, 243–255, 2004.
- McTainsh, G. H., Nickling, W. G., and Lynch, A. W.: Dust deposition and particle size in Mali, West Africa, *Catena*, 29, 307–322, 1997.
- 30 Mercone, D., Thomson, J., Croudace, I. W., Siani, G., Paterne, M., and Troelstra, S.: Duration of S1, the most recent sapropel in the eastern Mediterranean Sea, as indicated by accelerator mass spectrometry radiocarbon and geochemical evidence, *Paleoceanography*, 15, 336–347, 2000.

Atmospheric supply

V. Bout-Roumazeilles et al.

[Title Page](#)[Abstract](#)[Introduction](#)[Conclusions](#)[References](#)[Tables](#)[Figures](#)[◀](#)[▶](#)[◀](#)[▶](#)[Back](#)[Close](#)[Full Screen / Esc](#)[Printer-friendly Version](#)[Interactive Discussion](#)

Atmospheric supply

V. Bout-Roumazeilles et al.

[Title Page](#)[Abstract](#)[Introduction](#)[Conclusions](#)[References](#)[Tables](#)[Figures](#)[|◀](#)[▶|](#)[◀](#)[▶](#)[Back](#)[Close](#)[Full Screen / Esc](#)[Printer-friendly Version](#)[Interactive Discussion](#)

Atmospheric supply

V. Bout-Roumazeilles et al.

[Title Page](#)[Abstract](#)[Introduction](#)[Conclusions](#)[References](#)[Tables](#)[Figures](#)[◀](#)[▶](#)[◀](#)[▶](#)[Back](#)[Close](#)[Full Screen / Esc](#)[Printer-friendly Version](#)[Interactive Discussion](#)

Atmospheric supply

V. Bout-Roumazeilles et al.

[Title Page](#)[Abstract](#)[Introduction](#)[Conclusions](#)[References](#)[Tables](#)[Figures](#)[◀](#)[▶](#)[◀](#)[▶](#)[Back](#)[Close](#)[Full Screen / Esc](#)[Printer-friendly Version](#)[Interactive Discussion](#)

- Roberts, N., Brayshaw, D., Kuzucuoglu, C., Perez, R., and Sadori, L.: The mid-Holocene climatic transition in the Mediterranean: causes and consequences, *Holocene*, 21, 3–14, 2011.
- Rodriguez, S., Querol, X., Alastuey, A., Kallos, G., and Kakaliagou, O.: Saharan dust contributions to PM10 and TSP levels in Southern and Eastern Spain, *Atmos. Environ.*, 35, 2433–2447, 2001.
- Rohling, E. J.: Review and new aspects concerning the formation of eastern Mediterranean sapropels, *Mar. Geol.*, 122, 1–28, 1994.
- Rossignol-Strick, M.: Mediterranean Quaternary sapropels, an immediate response to the African monsoon to variation of insolation, *Paleogeogr. Palaeoecol.*, 49, 237–263, 1985.
- Rossignol-Strick, M., Nesteroff, W., Olive, P., and Vergnaud-Grazzini, C.: After the deluge: Mediterranean stagnation and sapropel formation, *Nature*, 295, 105–110, 1982.
- Rouis-Zargouni, I., Turon, J.-L., Londeix, L., Essallami, L., Kallel, N., and Sicre, M.-A.: Environmental and climatic changes in the central Mediterranean Sea (Siculo-Tunisian Strait) during the last 30 ka based on dinoflagellate cyst and planktonic *foraminifera* assemblages, *Paleogeogr. Palaeoecol.*, 285, 17–29, 2010.
- Rouis-Zargouni, I., Tron, J. L., Londeix, L., Kallel, N., and Essallami, L.: The last glacial-interglacial transition and dinoflagellate cysts in the western Mediterranean sea, *C. R. Geosci.*, 344, 99–109, doi:10.1016/j.crte.2012.01.002, 2012.
- Sadori, L., Giraudi, C., Pettitti, P., and Ramrath, A.: Human impact at Lago di Mezzano (central Italy) during the Bronze Age: a multidisciplinary approach, *Quaternary Int.*, 113, 5–17, 2004.
- Sadori, L., Zanchetta, G., and Giardini, M.: Last Glacial to Holocene palaeoenvironmental evolution at Lago di Pergusa (Sicily, Southern Italy) as inferred by pollen, microcharcoal, and stable isotopes, *Quaternary Int.*, 181, 4–14, 2008.
- Sadori, L., Jahns, S., and Peyron, O.: Mid-Holocene vegetation history of the central Mediterranean, *Holocene*, 21, 117–129, 2011.
- Saliot, A.: The Mediterranean Sea. The Handbook of Environmental Chemistry, v.5, Water Pollution, Springer-Verlag, Berlin, 408 pp., 2005.
- Sánchez-Goñi, M. F., Cacho, I., Turon, J. L., Guiot, J., Sierro, F. J., Peypouquet, J.-P., Grimalt, J. O., and Shackleton, N.: Synchronicity between marine and terrestrial responses to millennial scale climatic variability during the last glacial period in the Mediterranean region, *Clim. Dynam.*, 19, 95–105, 2002.
- Sawlowicz, Z.: Iridium and other platinum-group elements as geochemical markers in sedimentary environments, *Paleogeogr. Palaeoecol.*, 104, 253–270, 1993.

Atmospheric supply

V. Bout-Roumazeilles et al.

[Title Page](#)[Abstract](#)[Introduction](#)[Conclusions](#)[References](#)[Tables](#)[Figures](#)[◀](#)[▶](#)[◀](#)[▶](#)[Back](#)[Close](#)[Full Screen / Esc](#)[Printer-friendly Version](#)[Interactive Discussion](#)

Atmospheric supply

V. Bout-Roumazeilles et al.

[Title Page](#)[Abstract](#)[Introduction](#)[Conclusions](#)[References](#)[Tables](#)[Figures](#)[|◀](#)[▶|](#)[◀](#)[▶](#)[Back](#)[Close](#)[Full Screen / Esc](#)[Printer-friendly Version](#)[Interactive Discussion](#)

pel S1: Stalagmite evidence from Corchia cave (Central Italy), Quaternary Sci. Rev., 26, 279–286, 2007.

Zanchetta, G., Sulpizio, R., Roberts, N., Cioni, R., Eastwood, W. J., Siani, G., Caon, B., Paterne, M., and Santacroce, R.: Tephrostratigraphy, chronology and climatic events of the Mediterranean basin during the Holocene: An overview, Holocene, 21, 33–52, 2011.

5

Zielhofer, C. and Faust, D.: Mid- and Late Holocene fluvial chronology of Tunisia, Quaternary Sci. Rev., 27, 580–588, 2008.

CPD

8, 2921–2968, 2012

Atmospheric supply

V. Bout-Roumazeilles et al.

[Title Page](#)

[Abstract](#)

[Introduction](#)

[Conclusions](#)

[References](#)

[Tables](#)

[Figures](#)

◀

▶

◀

▶

[Back](#)

[Close](#)

[Full Screen / Esc](#)

[Printer-friendly Version](#)

[Interactive Discussion](#)



Atmospheric supply

V. Bout-Roumazeilles et al.

[Title Page](#)[Abstract](#)[Introduction](#)[Conclusions](#)[References](#)[Tables](#)[Figures](#)[◀](#)[▶](#)[◀](#)[▶](#)[Back](#)[Close](#)[Full Screen / Esc](#)[Printer-friendly Version](#)[Interactive Discussion](#)

Table 1. Radiocarbon ages performed on core MD04-2797. The ages were corrected using reservoir ages of 400 yr during the Holocene, the Younger Dryas and late glacial, 560 yr during the Bølling-Allerød and 800 yr during the Heinrich event H1 and the Older Dryas, following recommendations of Siani et al. (2001).

Depth (cm)	Species	¹⁴ C age (yr BP)	Error $\pm 1\sigma$	Corrected age (yr BP)	Error $\pm 1\sigma$	Calibrated age (cal yr BP)	Error $\pm 1\sigma$	Laboratory
0	<i>G. inflata</i>	1105*	20	705	20	668	9	ARTEMIS
80	foraminifera	5496	95	5093	95	5827	144	ARTEMIS
160	foraminifera	6700	85	6300	85	7241	120	ARTEMIS
199	foraminifera	7523	81	7123	81	7967	71	ARTEMIS
240	foraminifera	8113	81	7713	81	8488	98	ARTEMIS
330	<i>G. ruber</i>	8888	110	8488	110	9477	112	ARTEMIS
410	foraminifera	10 863	32	10 463	32	12 493	49	ARTEMIS
470	<i>G. inflata</i>	12 728	173	12 168	172	14 016	35	ARTEMIS
510	<i>G. ruber</i>	13 900	141	13 100	141	15 934	621	ARTEMIS
610	<i>G. ruber</i>	15 590	50	15 190	50	18 725	370	ARTEMIS
700	foraminifera	17 660	70	17 260	70	20 414	180	ARTEMIS
940	foraminifera	23 415	163	23 015	163	27 879	331	ARTEMIS
1030	foraminifera	26 095	7	25 695	7	30 490	156	ARTEMIS

* Data from Rouis-Zargouni et al. (2010).

Atmospheric supply

V. Bout-Roumazeilles et al.

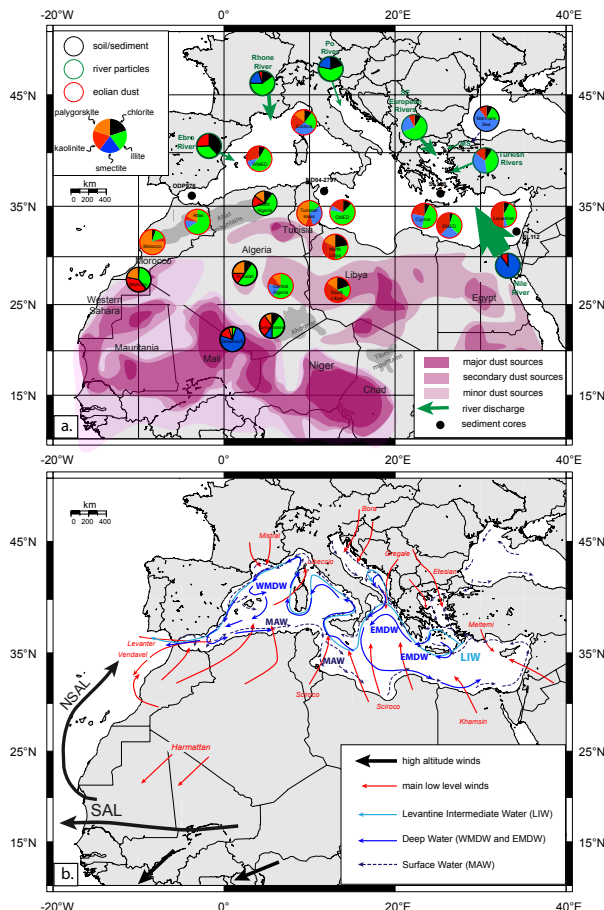
[Title Page](#)[Abstract](#)[Introduction](#)[Conclusions](#)[References](#)[Tables](#)[Figures](#)[|◀](#)[▶|](#)[◀](#)[▶](#)[Back](#)[Close](#)[Full Screen / Esc](#)[Printer-friendly Version](#)[Interactive Discussion](#)

Fig. 1. Caption on next page.

Atmospheric supply

V. Bout-Roumazeilles et al.

Fig. 1. Geographical settings: **(a)** clay mineralogy of peri-Mediterranean river particles (green circles), sediments/soils (black circles) and dust particles (red circles), modified from Bout-Roumazeilles et al. (2007), additional data from Cyprus and Levantine Sea: e.g. Hamann et al. (2009); data from northwest Aegean province and West Turkey province: e.g. Ehrmann et al. (2006); data from Marmara Sea: Armynot du Châtelet et al. (2012); North and South Libya dust from O'Hara et al. (2006). Position of the sediment cores mentioned in this study. Major, secondary and minor dust sources modified from D'Almeida (1998); Brooks and Legrand (2000); Caquineau et al. (2002); Prospero et al. (2002); Israelevich et al. (2002); Goudie (2003); Formenti et al. (2011a, b). Main low level (red arrows) and altitude winds (black arrows), rivers supply (green arrows, thickness proportional to annual suspended supply) in the Mediterranean Sea. SAL: Saharan Air Layer, NSAL: northern branch of the Saharan Air Layer. The limit between Sahara and Sahel is reported. Main surface (MAW), intermediate (Levantine Intermediate Water, LIW) and deep water (WMDW and EMDW) masses (Saliot, 2005).

[Title Page](#)[Abstract](#)[Introduction](#)[Conclusions](#)[References](#)[Tables](#)[Figures](#)[|◀](#)[▶|](#)[◀](#)[▶](#)[Back](#)[Close](#)[Full Screen / Esc](#)[Printer-friendly Version](#)[Interactive Discussion](#)

Atmospheric supply

V. Bout-Roumazeilles et al.

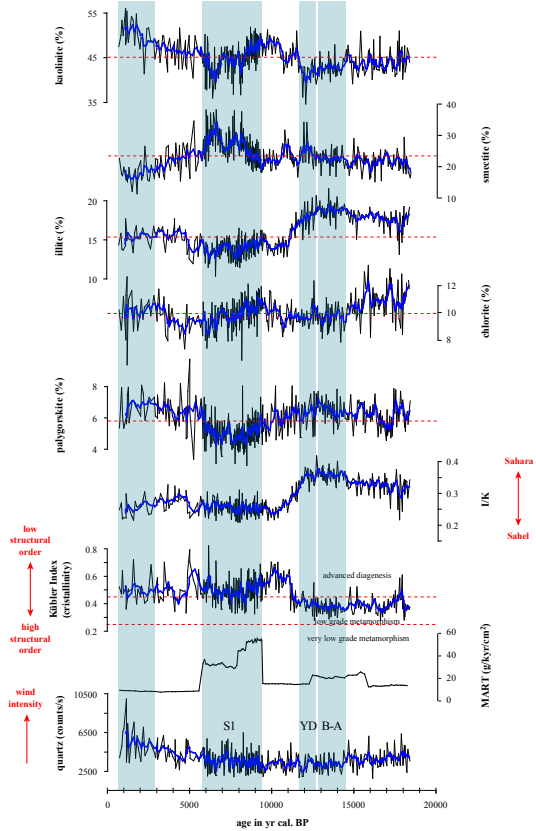


Fig. 2. Clay mineralogy of core MD04-2797: kaolinite (%), smectite (%), illite (%), chlorite (%), palygorskite (%), I/K : illite to kaolinite ratio, Kübler index (crystallinity), (MART) Terrigenous Mass Accumulation Rates ($\text{g kyr}^{-1} \text{cm}^{-2}$) and quartz content (counts/s) for the last 20 000 yr. B-A = Bølling-Allerød, YD = Younger Dryas, S1 = sapropel S1 (Mercone et al., 2000).

[Title Page](#)[Abstract](#)[Introduction](#)[Conclusions](#)[References](#)[Tables](#)[Figures](#)[|◀](#)[▶|](#)[◀](#)[▶](#)[Back](#)[Close](#)[Full Screen / Esc](#)[Printer-friendly Version](#)[Interactive Discussion](#)

Atmospheric supply

V. Bout-Roumazeilles et al.

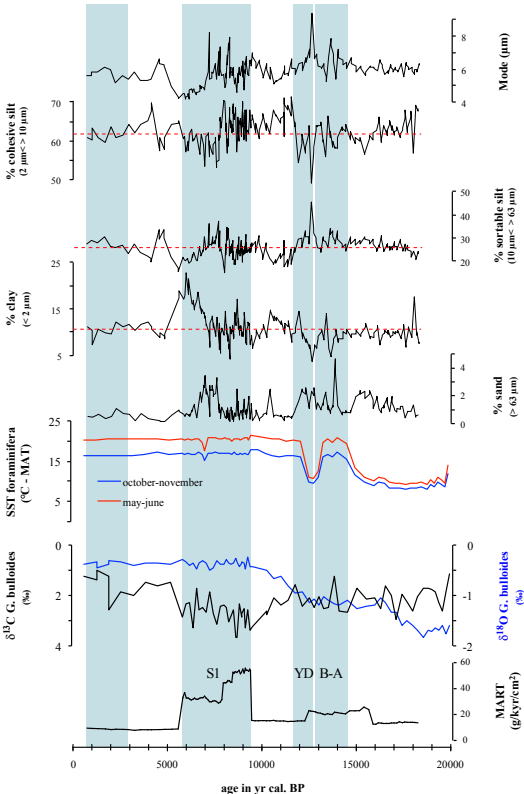


Fig. 3. Grain size analysis of core MD04-2797: mode (μm), % of cohesive silt ($2 < > 10 \mu\text{m}$), % of sortable silt ($10 < > 63 \mu\text{m}$), % of clay ($< 2 \mu\text{m}$) and % of sand ($> 63 \mu\text{m}$). MART from Fig. 1. Sea Surface Temperatures (SST) for May–June and October–November based on *foraminifera* association (Essallami et al., 2007), $\delta^{18}\text{O}$ (‰) and $\delta^{13}\text{C}$ from planktonic *foraminifera* *G. bulloides* (Essallami et al., 2007).

[Title Page](#)[Abstract](#)[Introduction](#)[Conclusions](#)[References](#)[Tables](#)[Figures](#)[|◀](#)[▶|](#)[◀](#)[▶](#)[Back](#)[Close](#)[Full Screen / Esc](#)[Printer-friendly Version](#)[Interactive Discussion](#)

Atmospheric supply

V. Bout-Roumazeilles et al.

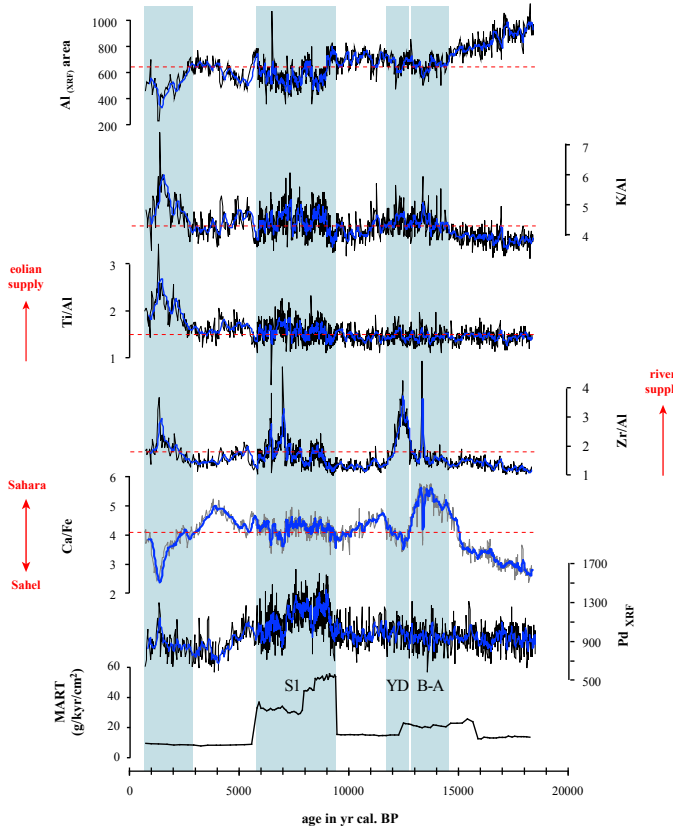


Fig. 4. Geochemical data for core MD04-2797, Al content (counts/s), Ti/Al ratio, Zr/Al ratio, Ca/Fe ratio and Pd content (counts/s). MART from Fig. 1.

Atmospheric supply

V. Bout-Roumazeilles et al.

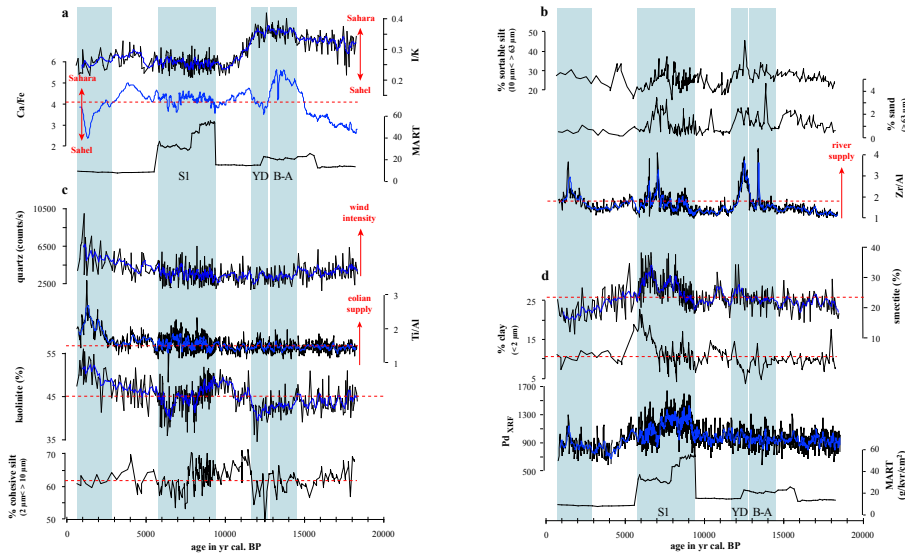


Fig. 5. Comparison of multiproxy data, **(a)**: I/K, Ca/Fe and their interpretation on particles provenance for the Bølling-Allerød, **(b)**: grain-size compared with Zr/Al during the Younger Dryas, **(c)**: quartz content (counts/s), Ti/Al ratio and kaolinite % over the last 3000 yr, **(d)**: Smectite (%), characterizing the sapropel S1, % of clay, content in Pd (counts/s) and MART.

[Title Page](#)[Abstract](#)[Introduction](#)[Conclusions](#)[References](#)[Tables](#)[Figures](#)[◀](#)[▶](#)[◀](#)[▶](#)[Back](#)[Close](#)[Full Screen / Esc](#)[Printer-friendly Version](#)[Interactive Discussion](#)

Atmospheric supply

V. Bout-Roumazeilles et al.

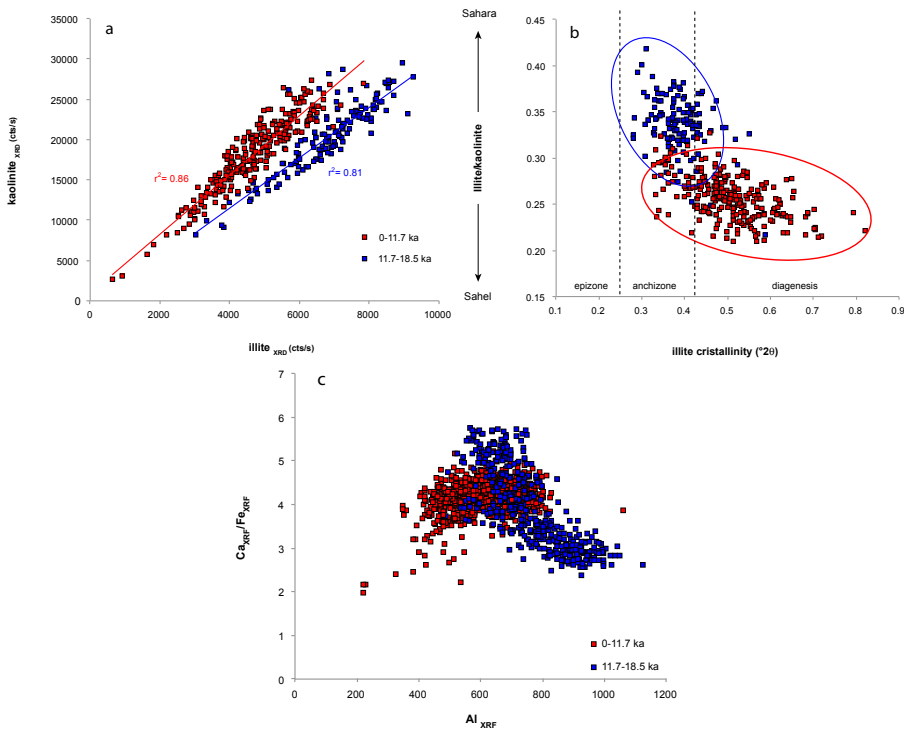


Fig. 6. Comparison of the mineralogical and geochemical signatures before and after 11.7 kyr, (a): kaolinite versus illite (XRD counts/s) evidencing contrasting provenance between 18.5 and 11.7 ka (red squares) and between 11.7 ka and top of the core (blue squares); (b): illite to kaolinite ratio as a function of illite crystallinity (Kübler Index), diagenesis, epizone and anchizone limits, (c): Ca content versus Fe content (counts XRF).

[Title Page](#)[Abstract](#)[Introduction](#)[Conclusions](#)[References](#)[Tables](#)[Figures](#)[|◀](#)[▶|](#)[◀](#)[▶](#)[Back](#)[Close](#)[Full Screen / Esc](#)[Printer-friendly Version](#)[Interactive Discussion](#)

Atmospheric supply

V. Bout-Roumazeilles et al.

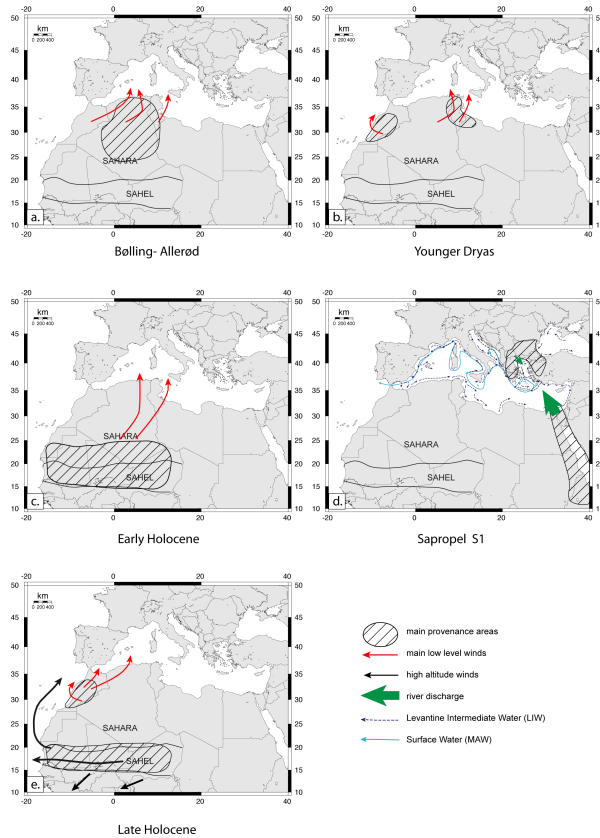
[Title Page](#)[Abstract](#)[Introduction](#)[Conclusions](#)[References](#)[Tables](#)[Figures](#)[|◀](#)[▶|](#)[◀](#)[▶](#)[Back](#)[Close](#)[Full Screen / Esc](#)[Printer-friendly Version](#)[Interactive Discussion](#)

Fig. 7. Main provenance (dashed areas) and potential eolian – low level (red arrows) or altitude winds (black arrows) – and riverine (green arrows) transportation patterns of clay-mineral particles for 5 timeslices, **(a)** Bølling-Allerød; **(b)** Younger Dryas; **(c)** early Holocene; **(d)** Sapropel S1; **(e)** late Holocene.